Journal of
Marine Science and Engineering

MDPI

Article

Laboratory Testing to Research the Micro-Structure and Dynamic Characteristics of Frozen–Thawed Marine Soft Soil

Zhi Ding [1], Bowen Kong [2,*], Xinjiang Wei [1], Mengya Zhang [1], Baolong Xu [1] and Fangjie Zhao [1]

[1] Department of Civil Engineering, Zhejiang University City College, Hangzhou 310015, China; dingz@zucc.edu.cn (Z.D.); weixj@zucc.edu.cn (X.W.); xuforest7@gmail.com (M.Z.); 31703023@stu.zucc.edu.cn (B.X.); zfj11mark3@gmail.com (F.Z.)

[2] Research Center of Coastal and Urban Geotechnical Engineering, College of Architecture and Civil Engineering, Zhejiang University, Hangzhou 310015, China

* Correspondence: kbw@zju.edu.cn; Tel.: +86-0571-88018968

Received: 30 January 2019; Accepted: 15 March 2019; Published: 27 March 2019

Abstract: The use of artificial freezing can change the mechanical properties of marine clay. In the construction of cross passages in metro tunnels in which the artificial ground freezing (AGF) method is applied, freeze–thaw circulation and cyclic loading could weaken the engineering properties of the clay, thus resulting in differential settlement. In this paper, the authors studied the dynamic properties of frozen–thawed soils under cyclic loading, with the help of dynamic triaxial testing. According to the dynamic triaxial test results and the images from scanning electron microscopy (SEM), the authors explained the weakening effect of both the freeze–thaw cycle and dynamic loading on soft soil. After freezing, the number of large pores increased. In addition, after cyclic loading, the pore structure of the soil showed a tendency towards compaction, which led to the large pores breaking into small ones. Subsequently, the potential reasons for the change of macroscopic dynamic characteristics were explained from a micro-scale point of view.

Keywords: marine soft soil; AGF; frozen–thawed cycle; dynamic triaxial test; cyclic loading; SEM; micro-structure

1. Introduction

The artificial ground freezing (AGF) method is normally used for the construction of tunnels in soft soil areas, especially in coastal regions such as Shanghai in China. The freeze–thaw cycle seriously alters the internal structure of the soil. Changes in microstructure characteristics affect the macroscopic properties of the soil. For now, the mechanism of a tunnel's long-term settlement under both freeze–thaw cycles and metro loading remains unclear. A further study on the dynamic properties of frozen–thawed soil is necessary, as this can provide the basis for controlling long-term settlements after AGF-method construction.

Engineered freezing–thawing soils are different from freezing–thawing soils in nature [1–4]. The phase changes between liquid and solid water in soil during a freeze–thaw period have been studied previously [5]. There are a variety of factors that influence the characteristics of frozen–thawed soil. Firstly, the type of soil—which includes moisture content [6–9] and pore morphology [10,11]—is a critical factor of the soil characteristics. Zhai et al. [12] found that, for consecutive freeze–thaw cycles, the proportion of micro-pores and mini-pores gradually decreased, while that of meso-pores and macropores increased. Watanabe et al. [13] point out that the effects of macropores on soil freezing and thawing with infiltration will lead to a unique distribution of water content. Leroueil et al. [14] found that the shear stress peak value of over-consolidated clay became significantly lower after

freeze–thaw cycles. Chamberlain et al. [15] found that, due to the freeze–thaw action, the porosity of the soil decreased, while the permeability of the soil increased. The permeability coefficient of the soil increased by one to two orders after the freeze–thaw cycle [16]. The authors' explanation for this is that the micro-fissures which develop in the process of freeze–thaw cycles cause the permeability coefficient to increase. Viklander et al. [17] found that the change of soil density after the freeze–thaw cycle was related to the soil properties. After the freeze–thaw cycle, the porosity ratio of dense soil increased, while the porosity ratio of loose soil decreased. The porosity ratio after several freeze–thaw cycles of soil approaches the same pore ratio, called the residual porosity. Sangrey et al. [18] carried out a study on the relationship between effective stress and strain pore pressure. Several simulation models were developed to explore the mechanism of frozen soil [19] and evaluate the thaw settlement after artificial ground freezing [20]. He et al. [21] compared various dynamic responses of thawing soil and undisturbed soil using the numerical simulation method.

Furthermore, the triaxial test [22], especially the dynamic triaxial test, is widely used in soil-performance analysis. Leroueil et al. [14] presented the mechanical behaviors of Champlain sea clay under a single freeze–thaw cycle by triaxial test and suggest that most of the soil characteristics are related to the initial liquidity index of the soil. Graham et al. [23] found that the soil structure was severely damaged after cyclic loading and that the compression curve of remolded clay roughly coincided with that of undisturbed soil. Kazuya et al. [24] conducted a three-axis cyclic experiment on stress-controlled soft clay, suggesting that the normalized pore pressure had a hyperbolic relationship with the cyclic shear strain. Larew et al. [25] proposed a critical cyclic stress ratio, where the soft clay would not be damaged unless the cyclic stress exceeds the critical stress ratio value. Hui et al. [6] worked on the redistribution of water and salt in soil under cyclical freeze–thaw. Zhang et al. [26] investigated the variation of the microscopic pore structures of silty clay samples before and after freezing–thawing under cyclic loading.

Referring to the studies above, it can be predicted that the dynamic characteristics of soft soil will reduce after freeze–thaw cycles, resulting in a large degree of deformation under dynamic loading. The change of microstructure characteristics is the essence of macroscopic behavioral change. The microstructure of soil is mainly described by the morphology and arrangement of soil particles and pores [27], but the arrangement of soft soil particles is complicated and random. The structural elements are in a complex dynamic equilibrium under freeze–thaw cycles and dynamic loading [28,29]. To explore the law of frozen–thawed soil settlement under dynamic loading, this paper used microstructure parameters to quantitatively analyze the dynamic characteristics in changes of soils with the help of a dynamic triaxial test machine and scanning electron microscopy (SEM).

2. Materials and Methods

2.1. Remolded Soil Samples

The soil samples were taken from the Hangzhou Metro Line 2 Liangzhu station. For undisturbed soil, the total unit weight is 17.6 kN/m^3, the water content ω is 47%, the grain density ϱs is 2.74 g/cm^3, the plastic limit is 31.4%, the liquid limit is 49.2%, and the plasticity index is 17.8. The preparation of remolded soil was based on the multi-channel intelligent remolded soil vacuum preloading equipment (Figure 1). The vacuum container invented by Sheahan et al. [22] was used to make soil samples. The uniformity of the remolded soil is demonstrated. For the remolded soil, which is shown in Figure 2, the unit weight is 18.2 kN/m^3, grain density ϱs is 2.74 g/cm^3, remolded water content $\omega$is 45%, plastic limit is 33.4%, liquid limit is 51.6%, and the plasticity index is 18.2.

The frozen–thawed soil samples were prepared in a cylinder with a 38-mm diameter and a 76-mm height which was then placed into a vacuum saturation cylinder and vacuumed at −0.1 MPa (relative to atmospheric pressure) for 3 h and finally submerged in water at atmospheric pressure for 12 h to saturate the soil samples.

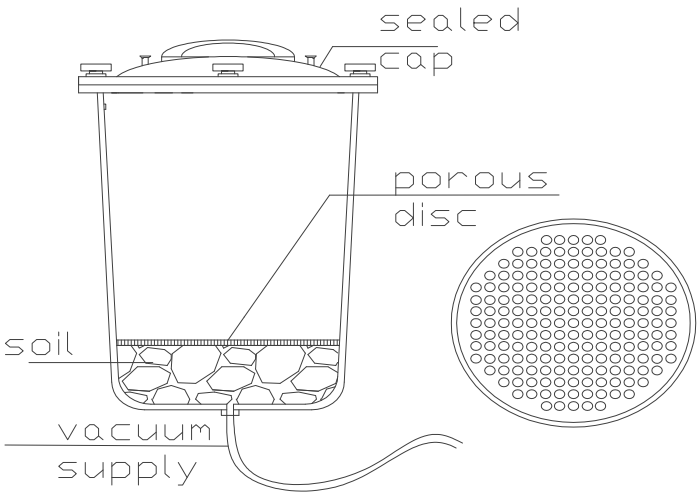

Figure 1. Vacuum preloading equipment.

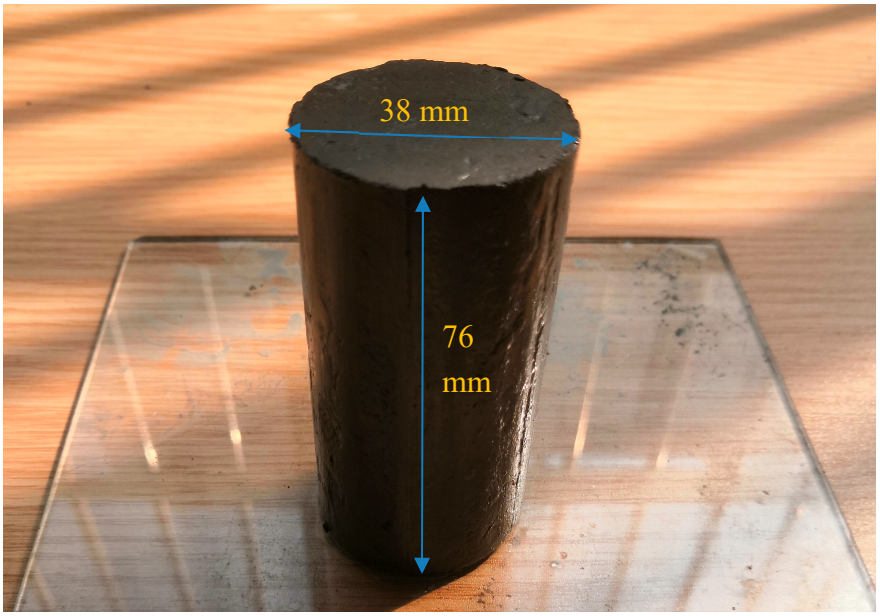

Figure 2. Remolded soil sample.

2.2. Cyclic Loading

A bias-sine wave was used to simulate the subway loads. The effective consolidation stress was selected as p = 200 kPa (the confining pressure was 550 kPa, and the back pressure was 350 kPa), and the cyclic stress ratio $\tau = \sigma_d/2p$ (σ_d is the static deviator stress) was selected as 0.2. The static deviator stress was selected as 40 kPa. To simulate the long-term cyclic loading on the soil during subway operations, 20,000 times loading was chosen. The authors selected 1 Hz for the frequency of cyclic loading [30], and the loading was applied by the dynamic triaxial test machine invented by GDS (Geotechnical Digital Systems) company (Hook, UK) in Figure 3. The components of the dynamic triaxial test machine and waveform are shown in Figure 4. The saturation and consolidation stage can be achieved by the pressure controllers. The software designed by GDS company called GDSlab v2.5.4.5.

Figure 3. Dynamic triaxial test machine.

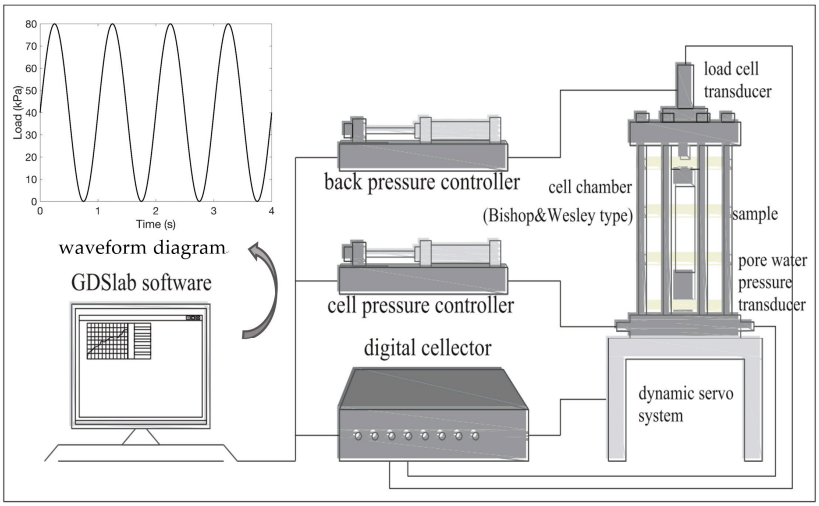

Figure 4. Components of the dynamic triaxial test machine.

2.3. Freeze–Thaw Cycles

In the process of subway construction, the design temperature of the frozen wall is −20 °C, while the cooling medium is about −30 °C. In terms of the freezing temperature, the remolded clay was frozen for 48 h at −30 °C, −20 °C, and −10 °C. In exceptional construction situations, the foundation soil could be frozen twice. For this reason, 0 to 2 freeze-thaw cycles were set for the comparative test. For the 76-mm high frozen remolded clay, 48 h is a suitable freezing time to simulate practical engineering. In one freeze–thaw cycle, the remolded clay was frozen at the set experimental temperature for 48 h in a low-temperature freezing box, then thawed in the chamber with constant temperature and humidity for another 48 h.

2.4. Microscopic Observation

The SEM technique is one of the main methods to investigate the surface structure of materials that can also be applied to soils [31] and rocks [32]. In this paper, the field-emission scanning electron microscope (FES 650) in Figure 5 was adopted for soil surface analysis. The remolded soil samples were cut into strips with a 2 cm × 2 cm cross-section. After drying, the remolded soil strips were broken every 2 cm along their height for observation. To ensure the quality of the micro-images, the authors coated the dry soil surface with a layer of 20–50 nm gold film as a conductive material (Figure 6). All pictures of the soil sample were at 8000 times magnification, and the representative regions were continuously photographed 15 times.

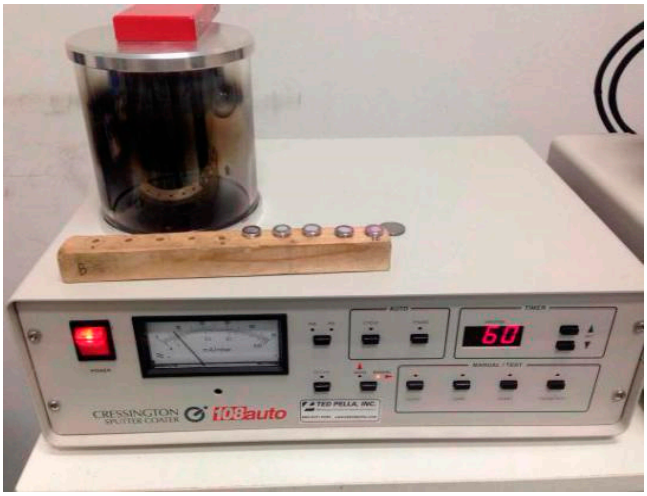

Figure 5. Field-emission scanning electron microscope.

Figure 6. Spraying conductive material microscopy.

2.5. Experimental Plan

The soil samples were frozen at −10 °C, −20 °C, and −30 °C. As shown in Table 1, seven samples were set. In addition, the microstructure changes of the frozen–thawed soil before and after freeze–thaw action were studied. During the experiment, GDSlab software was used to control pressure and cyclic loading while collecting data. All the data were recorded and displayed in real time.

Table 1. GDS experimental plan.

Number	Stress Ratio	Static Deviator Stress	Frequency	Temperature	Freeze–Thaw Cycle Times	Loading Cycle Times
		kPa	Hz	°C		
C-1	0.2	40	1	-	0	20,000
C-2	0.2	40	1	−30	1	20,000
C-3	0.2	40	1	−20	1	20,000
C-4	0.2	40	1	−10	1	20,000
C-5	0.2	40	1	−30	2	20,000
C-6	0.2	40	1	−20	2	20,000
C-7	0.2	40	1	−10	2	20,000

3. Qualitative Analysis of the Microstructure

3.1. Microstructure of Soil under a Freeze–Thaw Cycle

The particle morphology and pore shape of the soil was photographed by SEM. The aggregation structure in the red circle and fragment structure in the green circle can be observed in Figure 7, which shows the microstructure scan images of the unfrozen soil sample and the −10 °C frozen soil sample. During the freezing process, it can be inferred that the growth of ice crystals destroys the coupling effect between the soil particles. Thus, pores in the soil connected to others and turned into larger ones; then, a new soil skeleton structure formed. During melting, the disappearance of ice crystals cannot completely restore the original skeleton structure. It can be seen that the aggregation structures (red circle) play a dominant role in the soil skeleton before freezing; however, the fragment structure (green circle) takes the dominant role after thawing.

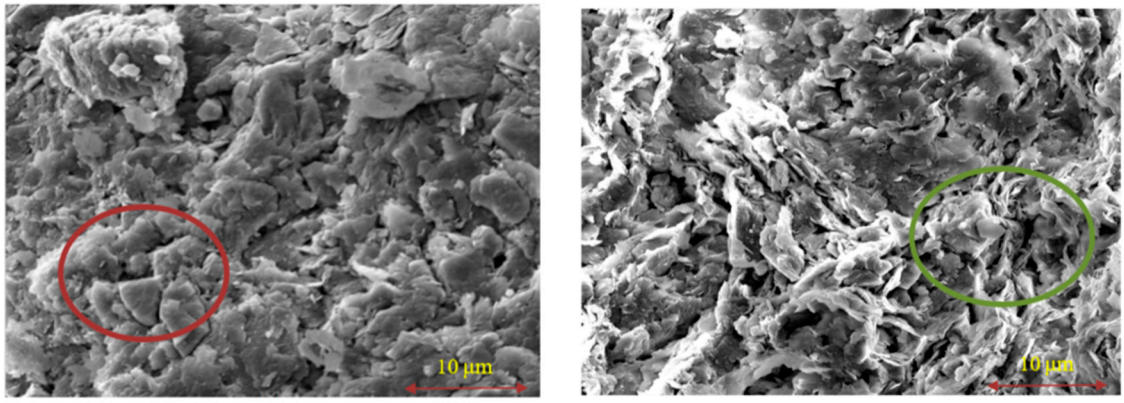

(**a**) (**b**)

Figure 7. SEM image: (**a**) unfrozen soil; (**b**) frozen soil at −10 °C.

After another freeze–thaw cycle, the weakening effect, shown by a looser structure, became more pronounced. It can be seen in Figure 8 that the dark parts of the SEM picture increase significantly after a second freeze–thaw cycle, shown at 8000 times magnification, and the fragment structure (green circle) became more obvious while the aggregation structures (red circle) decreased. The double frost heave damage on the second frozen soil exacerbated the breaking of the skeleton.

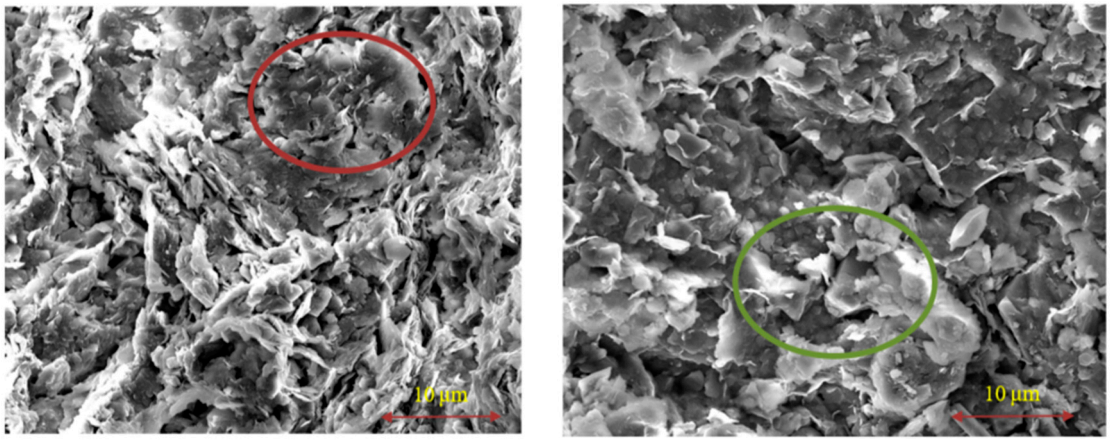

(**a**) (**b**)

Figure 8. SEM image: (**a**) one cycle frozen soil at −10 °C; (**b**) second cycle frozen soil at −10 °C.

The microstructure changes of soft soil shown in the images from electron microscopy scanning experiments were beneficial to explain the structural weakening mechanism of soft soil.

3.2. Microstructure of Frozen–Thawed Soil under Cycle Loading

Figure 9 reveals the frozen-thawed soil samples' structural changes before and after cyclic loading. It can be seen that the loose structure of frozen soil became compacted because of the cyclic loading. The predominance of platy structures (green circles) were replaced by agglomeration structures (yellow circles), indicating that the structure of the frozen soil became more stable after a long time of cyclic loading. It can be inferred that the adjacent soil particles were squeezed and aggregated, resulting in a denser soil skeleton structure. The compaction affection can improve the strength of the soft soil, but lead to uneven settlement.

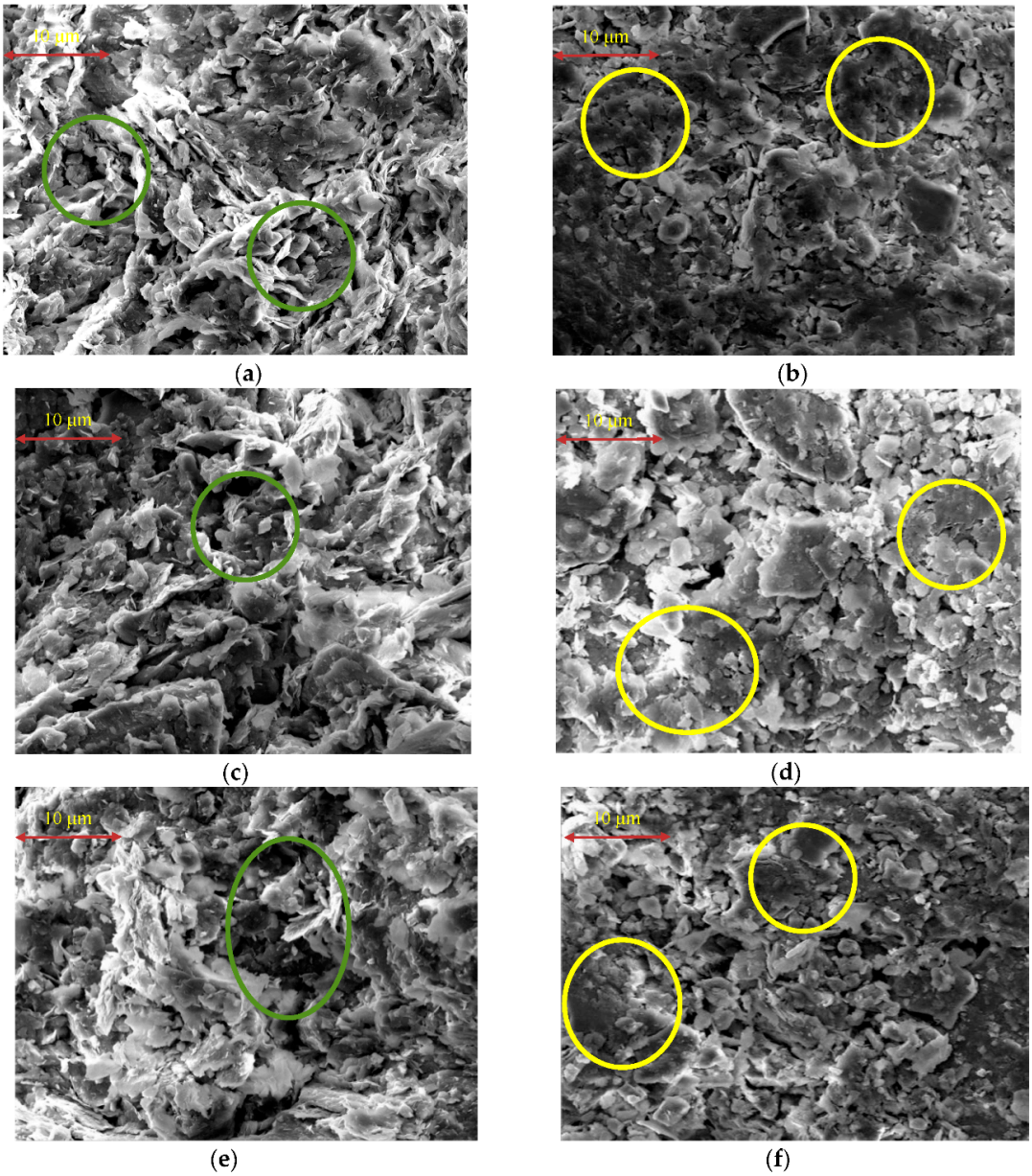

Figure 9. SEM images: (**a**) frozen–thawed soil at −10 °C before cyclic loading; (**b**) frozen–thawed soil at −10 °C after cyclic loading; (**c**) frozen–thawed soil at −20 °C before cyclic loading; (**d**) frozen–thawed soil at −20 °C after cyclic loading; (**e**) frozen–thawed soil at −30 °C before cyclic loading; (**f**) frozen–thawed soil at −30 °C after cyclic loading.

Figure 10 shows the scan images of first-cycle frozen soil and second-cycle frozen soil after cyclic loading. It is clear that the number of dense group structures in second-cycle frozen soil (purple rectangles) is more than that in once-frozen–thawed soil (light blue rectangles). On account of the more serious fragmentation for second-cycle frozen soil than first-cycle frozen soil, the second-cycle frozen soil had a denser structure than first-cycle frozen soil. From the enlargement of the average size of soil aggregates after a secondary freeze–thaw action, it could be deduced that the compacting effect of the soil particles became more evident.

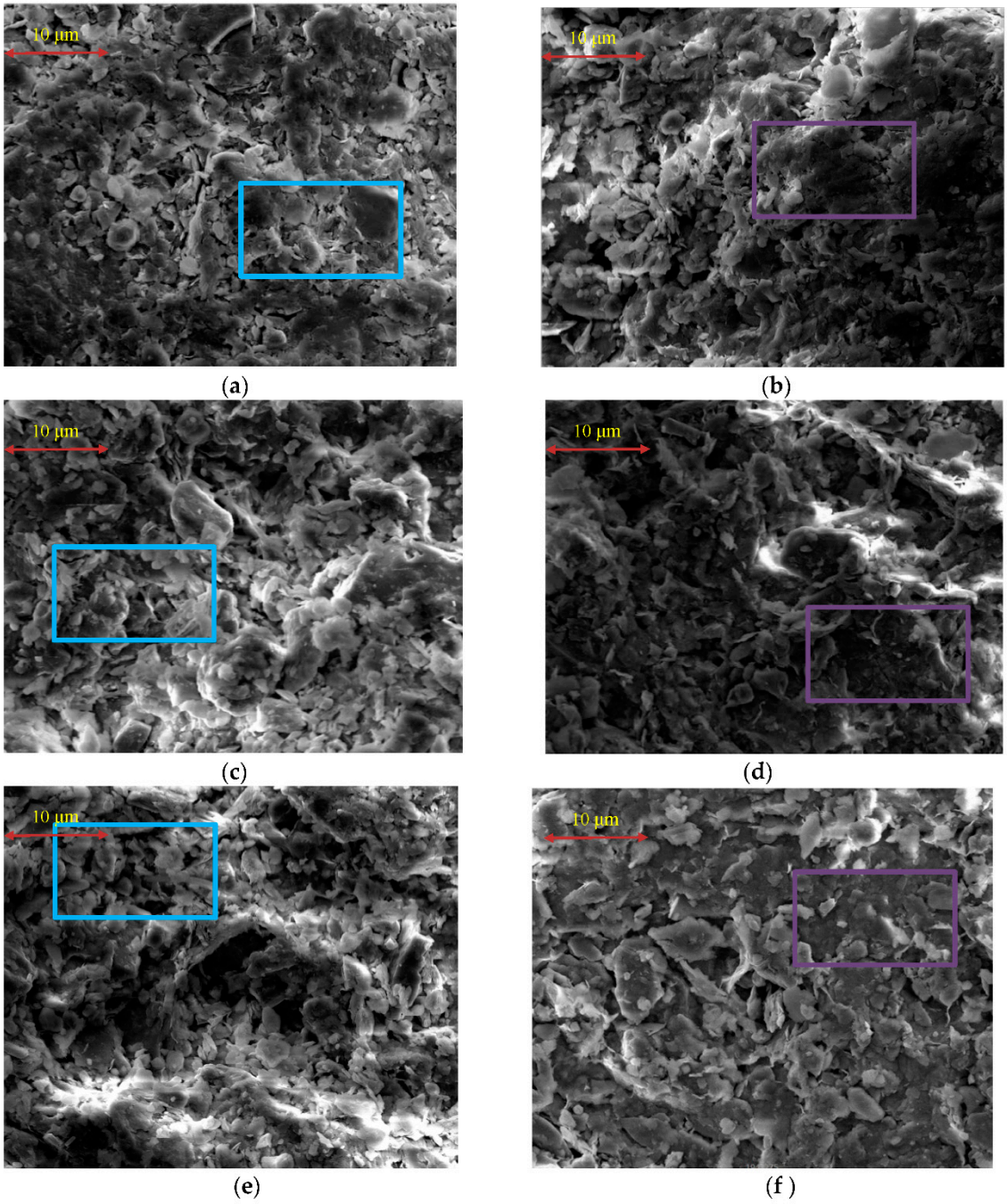

Figure 10. SEM images: (**a**) first-cycle frozen soil after cyclic loading at −10 °C; (**b**) second-cycle frozen soil after cyclic loading at −10 °C; (**c**) first-cycle frozen soil after cyclic loading at −20 °C; (**d**) second-cycle frozen soil after cyclic loading at −20 °C; (**e**) first-cycle frozen soil after cyclic loading at −30 °C; (**f**) second-cycle frozen soil after cyclic loading at −30 °C.

4. Quantitative Analysis of the Microstructure

4.1. Microstructure Analysis of Soil under Freeze–Thaw Cycles

In the SEM images, the pores around the agglomerate can be observed, but it is difficult to measure the pores' size. Therefore, the microphotograph was binarized by IPP (Image-Pro Plus) image analysis software (Figure 11) to calculate the pore size [28]. The white parts (blue circles in Figure 11) of the binary picture were considered to be pores. The initial choice of the gray scales has an influence on pore size; however, it has little influence on the percentage change of pores, which is more meaningful to the destruction mechanism.

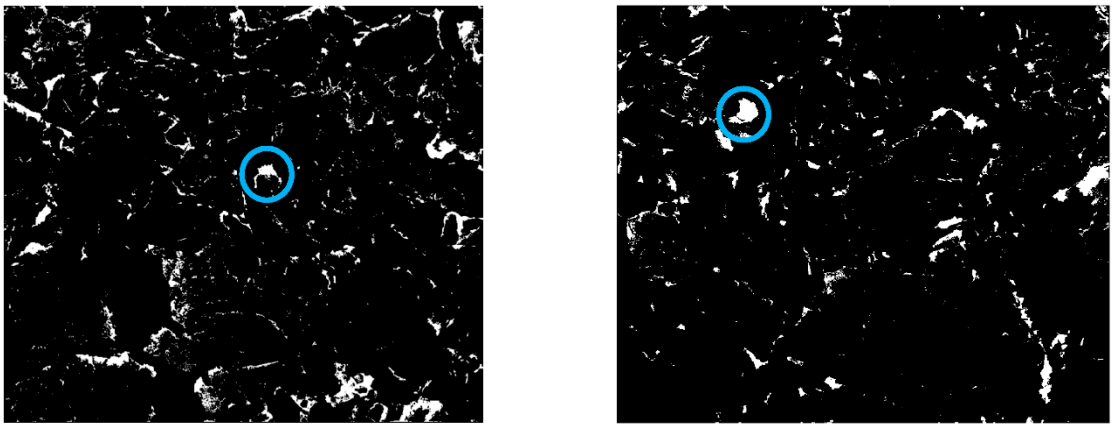

(**a**) (**b**)

Figure 11. Binarized scanning pictures: (**a**) unfrozen soil before cyclic loading; (**b**) unfrozen soil after cyclic loading.

4.1.1. Method and Parameters

The microstructure characteristic parameters can be identified and calculated by software, such as the diameter, area, perimeter, shape factor, and roundness. This sub-section selects the following characteristic parameters to analyze the changes in pore structure:

- The area corresponds to the area occupied by the outline of the object.
- Equivalent diameter (mean): After connecting two points on the outline of the selected object, this is calculated as the average value of the length of the line passing through the centroid.
- The fractal dimension is calculated by the area–circumference method. The basic principle is as follows:

$$\log(P) = (D/2)\log(A) + C \quad (1)$$

where P is the pore perimeter, A is the pore area, and D is the fractal dimension of the pore.

- Surface void ratio e_w: the ratio of pore area to particle area.

$$e_w = S_w/(S - S_w) \quad (2)$$

where S_w is the pore area, and S is the particle area.

4.1.2. Distribution of Pore Diameters after Freeze–Thaw Cycles

Figure 12 shows the distribution of pore diameters under different freezing temperatures. It is observed that the number of small pores (D = 0.3~0.5 μm) reduced, while the number of macro-pores (D > 1 μm) increased. Taking the −10 °C frozen soil as an example, the number of macro-pores nearly doubled after the freeze–thaw cycle. It can also be seen that the lower the freezing temperature, the smaller the percentage of small pores and the larger the percentage of the other two sized pores (D = 0.5~1 μm and D > 1 μm).

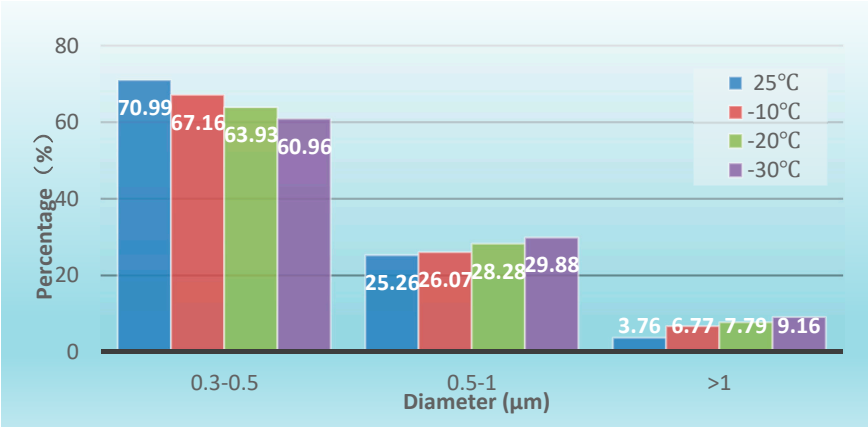

Figure 12. Distribution of the pore diameter under various temperatures.

Figure 13 shows the influence of the second freeze–thaw cycle on the pore diameter distribution of soft soil. There was the same trend of pore-distribution change as in first-cycle frozen soil. This trend became more obvious with the increase of the number of freeze–thaw cycles.

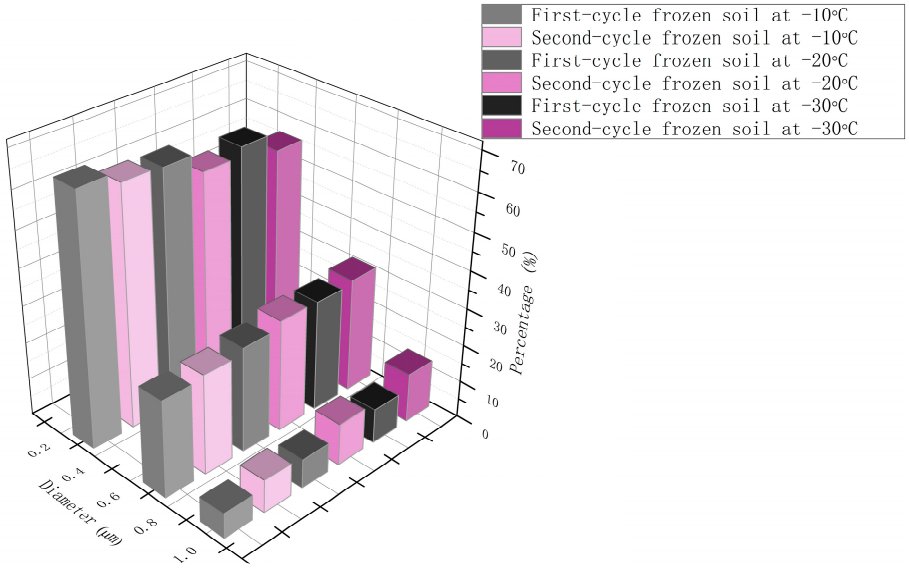

Figure 13. Distribution of the diameter under the second freeze–thaw cycle.

The first freeze–thaw cycle formed weakened areas in the soil structure. The second freeze–thaw cycle not only damaged these weakened areas, but also brought about new structural damage. It can be inferred that the added freezing action will aggravate the redistribution of particles, resulting in an increase in the number of large pores.

4.1.3. Distribution of Pore Area after Freeze-Thaw Cycles

Figure 14 shows the pore cumulative distribution curves of first and second-cycle frozen soils at different freezing temperatures. The steep development of the curves indicates that the pore area distribution is concentrated in the range of 0–1 μm^2. With the decrease of freezing temperature, the pore area cumulative distribution curve tends to move upwards, indicating that the proportion of large pores has increased.

Figure 15 shows the effect of the number of freeze–thaw cycles on the pore area accumulation curve. Taking −30 °C as an example, it can be seen that the curve shifts upwards after the second

freeze-thaw cycle. The potential reason for this trend is that the destructive effect of the frost heave on the structure continues to accumulate under the second freeze-thaw cycle.

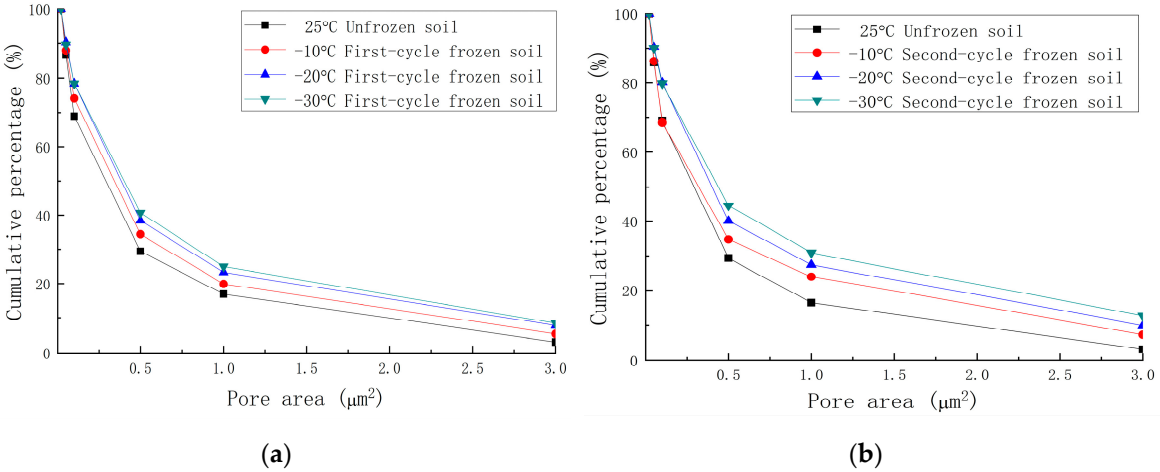

(**a**) (**b**)

Figure 14. Pore area distribution: (**a**) first-cycle frozen soil; (**b**) second-cycle frozen soil.

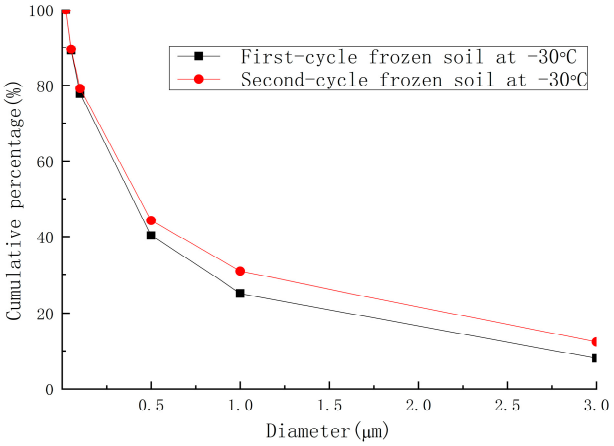

Figure 15. Pore area distribution of frozen soil at −30 °C.

4.1.4. Surface Void Ratio under Freeze–Thaw Cycles

Based on the concept of the void ratio, the concept of the surface void ratio (Equation (2)) was introduced into the microstructure. The surface void ratio was smaller than the three-dimensional porosity ratio, but it can be used as a two-dimensional parameter to represent the variation of the spatial pore volume. Table 2 shows the variation of the void ratio of soft soil after different freezing temperatures and freeze–thaw cycles. It can be seen that the surface void ratio has a tendency to increase after the freeze–thaw cycles. The change rule of the surface void ratio is consistent with the one of equivalent diameter, so the conclusion was mutually verified.

Table 2. Surface void ratio.

Sample	Unfrozen	T= −10 °C		T= −20 °C		T= −30 °C	
		First Cycle Frozen	Second Cycle Frozen	First Cycle Frozen	Second Cycle Frozen	First Cycle Frozen	Second Cycle Frozen
Surface void ratio	0.0364	0.0420	0.0483	0.0501	0.0586	0.0598	0.0697

4.1.5. Pore Fractal Dimensions under Freeze–Thaw Cycles

Fractal theory is used to describe the irregular shape degree of particles in the study of microstructure morphology. When the surface of the particle was relatively smooth, the value of fractal dimension D decreased.

Figure 16 shows that the average fractal dimension of the soft soil after freeze–thaw cycles was increased. In addition, the fractal dimension increased with the decrease of the freezing temperature. This indicated that, during the soft-water freeze–thaw cycle, the growth of ice crystals caused the tiny pores to become connected and turn into large ones with a more irregular shape.

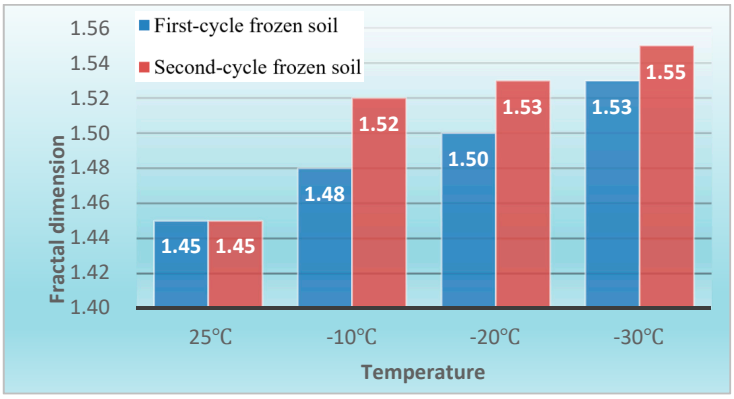

Figure 16. Average fractal dimension of soil pores.

4.2. Under Cyclic Loading

Figure 17 shows the equivalent diameter distribution of pores under various freezing temperatures and cyclic loading conditions. From the percentage of the pore diameters which fall between 0.3–0.5 μm and ≥0.5 μm, it can be seen that the number of large pores reduced, while the number of micro-pores increased after loading. This trend became more obvious after one more freeze–thaw cycle.

4.3. Accumulative Distribution of the Pore Area

Table 3 indicates the classification of the frozen–thawed soil's pore area before and after cyclic loading. It also shows that the percentage of micro-pores increased, while the percentage of macro-pores reduced after cyclic loading. The lower the freezing temperature, the more obvious this trend was. The results of area change coincided with the change rule of equivalent diameter.

Table 3. Distribution of pore area.

Area (μm²)			0.02–0.05	0.05–0.1	0.1–0.5	0.5–1	1–3	>3
First-cycle frozen Soil	−10 °C	B CL[1]	12.27%	13.55%	40.07%	14.15%	14.69%	5.28%
		A CL[2]	15.08%	16.90%	41.63%	12.97%	11.64%	1.77%
	−20 °C	B CL[1]	10.78%	12.28%	38.30%	14.70%	15.78%	8.16%
		A CL[2]	15.68%	17.25%	40.08%	13.71%	10.24%	3.04%
	−30 °C	B CL[1]	10.60%	11.30%	37.76%	15.18%	17.00%	8.15%
		A CL[2]	17.58%	20.32%	39.96%	12.93%	5.90%	3.31%
Second-cycle frozen Soil	−10 °C	B CL[1]	14.43%	17.22%	33.62%	10.61%	16.79%	7.32%
		A CL[2]	15.65%	16.20%	45.34%	10.71%	8.23%	3.86%
	−20 °C	B CL[1]	9.90%	10.12%	39.60%	12.91%	17.54%	9.93%
		A CL[2]	15.79%	18.79%	43.20%	10.91%	5.52%	5.79%
	−30 °C	B CL[1]	10.32%	10.31%	34.84%	13.46%	18.58%	12.49%
		A CL[2]	10.58%	12.82%	41.85%	12.86%	13.74%	8.15%

[1] Before cyclic loading; [2] After cyclic loading.

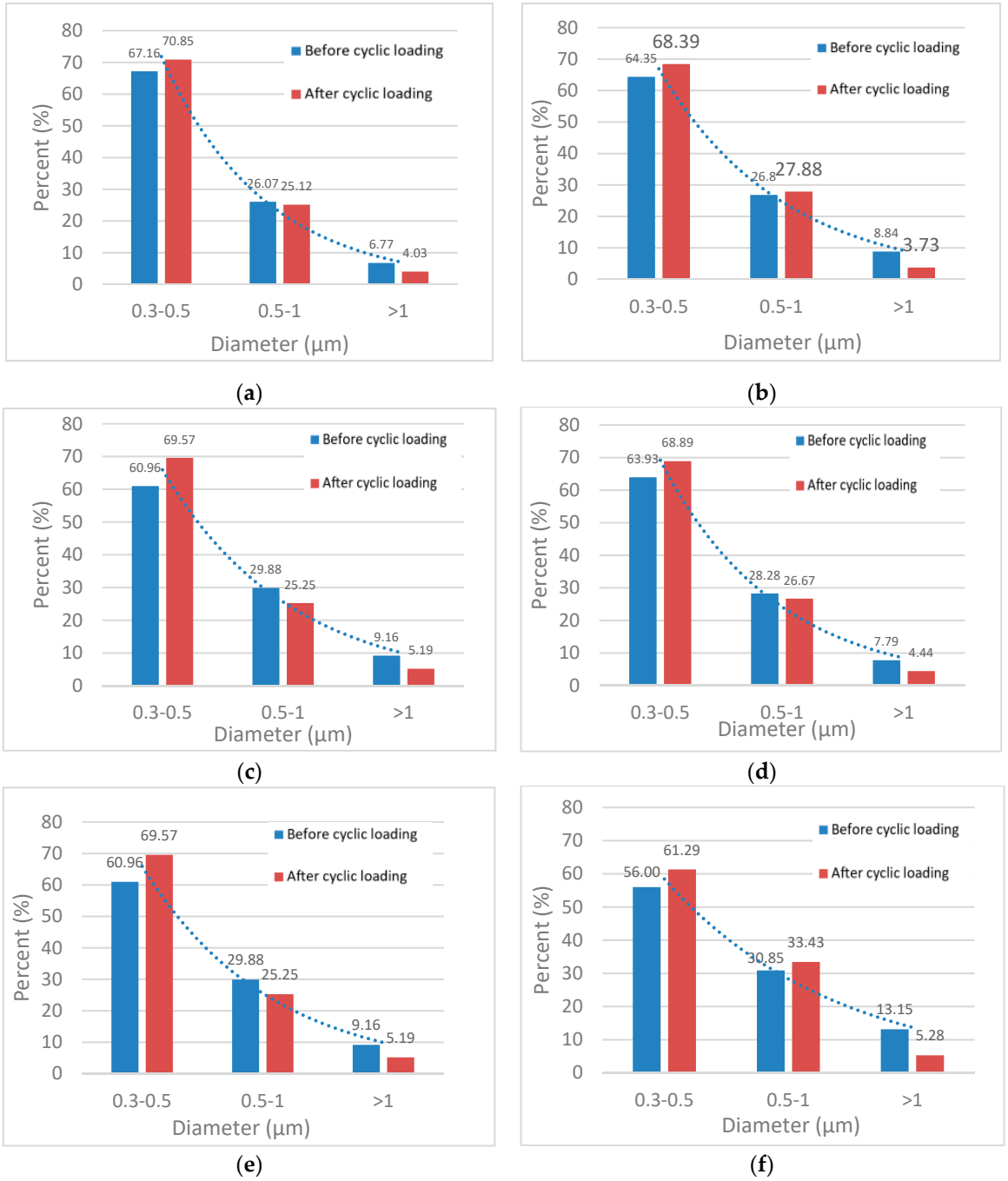

Figure 17. Distribution of effective pore size for (**a**) first-cycle frozen soil after cyclic loading at −10 °C; (**b**) second-cycle frozen soil after cyclic loading at −10 °C; (**c**) first-cycle frozen soil after cyclic loading at −20 °C; (**d**) second-cycle frozen soil after cyclic loading at −20 °C; (**e**) first-cycle frozen soil after cyclic loading at −30 °C; (**f**) second-cycle frozen soil after cyclic loading at −30 °C.

Figure 18 shows the cumulative distribution curves of the pore area before and after cyclic loading. The black curve stands for the sample before cyclic loading, and the red curve represents the sample after cyclic loading. The curves had a large slope in the range of ≤0.5 μm^2, which indicated that micro-pores were the most numerous of all pore types. Comparing the two curves in Figure 18a–f, it is found that cyclic loading reduced the number of large pores, and it was also revealed that the proportion of micro-pores increased while the proportion of macro-pores decreased. As the second freeze-thaw cycle was added, the compression effect became more obvious, as seen in Figure 18.

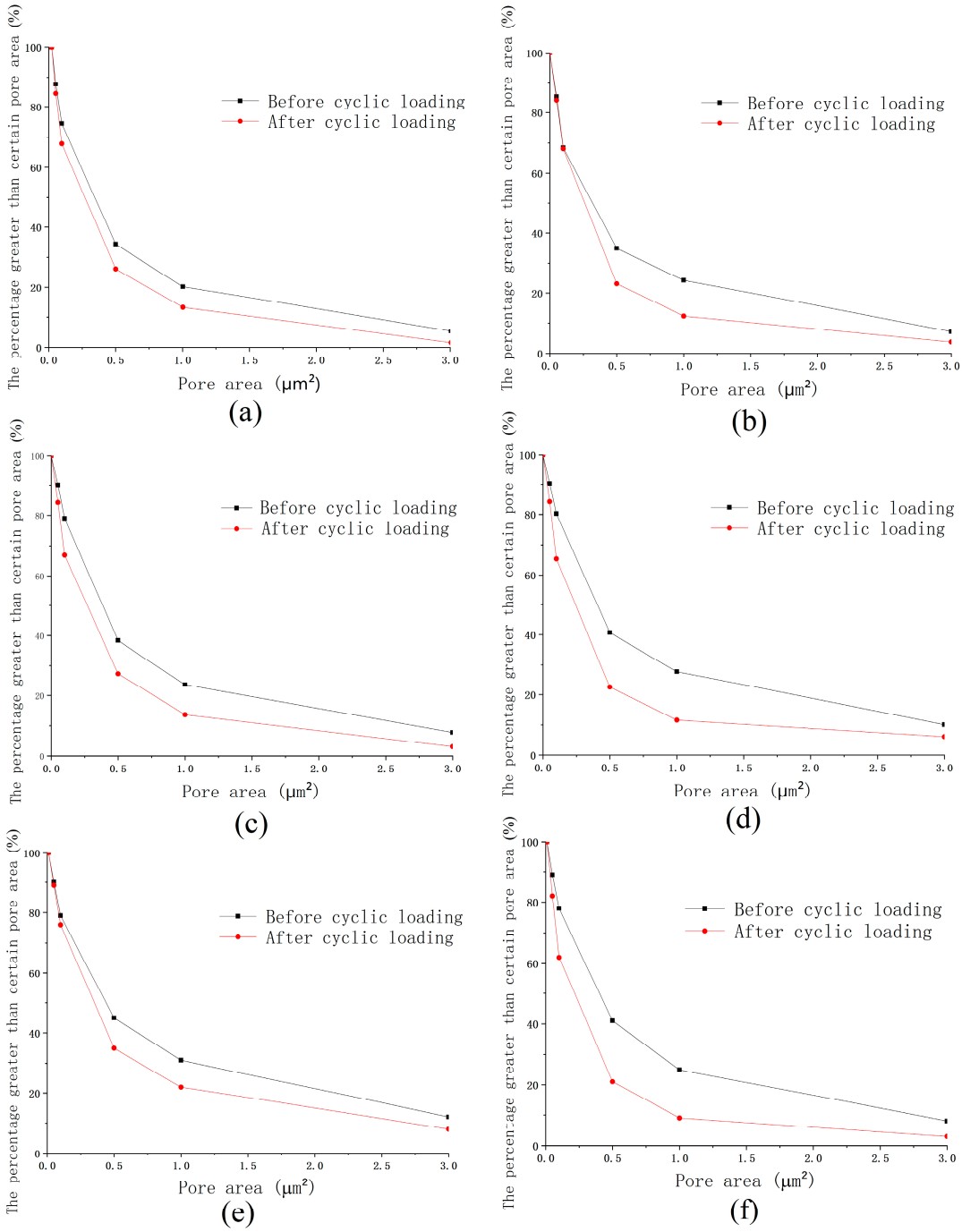

Figure 18. Cumulative distribution of pore area for (**a**) first-cycle frozen soil after loading at −10 °C; (**b**) second-cycle frozen soil after loading at −10 °C; (**c**) first-cycle frozen soil after loading at −20 °C; (**d**) second-cycle frozen soil after loading at −20 °C; (**e**) first-cycle frozen soil after loading at −30 °C; (**f**) second-cycle frozen soil after loading at −30 °C.

4.4. Changes of Pore Fractal Dimension

Table 4 confirms the change of pores' fractal dimensions in terms of the experimental result. The reduction of the fractal dimension manifests the complexity of the pore, which was reduced after cyclic loading. The redistribution of the grain skeleton because of cyclic loading made the pore distribution directional and uniform. In addition, the lower the freezing temperature, the more nonuniform the pore was.

Table 4. Fractal dimension of pores.

	First-Cycle Frozen Soil			Second-Cycle Frozen Soil		
Temperature	−10 °C	−20 °C	−30 °C	−10 °C	−20 °C	−30 °C
B CL[1]	1.4809	1.5003	1.5301	1.5211	1.5328	1.5531
A CL[2]	1.4103	1.4205	1.4548	1.4528	1.476	1.4991

[1] Before cyclic loading; [2] After cyclic loading.

5. Results and Discussion

5.1. Relationship of the Void Ratio and Axial Strain

From the SEM images, it is found that the nature of the weakening effect of the dynamic characteristics, such as pore pressure and axial strain before and after the freeze–thaw cycle, came from the microstructure rearrangement. Figures 19 and 20 show the correlation curves of the void ratio vs. axial strain and void ratio vs. normalized pore pressure (pore pressure divided by effective confining pressure) after cyclic loading. It can be observed from the figures that the axial strain and pore pressure increased at the same time as the increase of the pore ratio. Considering the freeze–thaw cycle at −30 °C as an example, the voids of the frozen soils increased by about 64%, the corresponding limit axial strain increased by 50%, and the pore pressure increased by about 27%.

The results pointed to the weakening mechanism of soft soil under freeze–thaw cycles: water phase transition due to the positive and negative temperature changes. The swelling frozen pore water squeezed the nearby soil particles, resulting in the destruction of the link between the particles. Then, the tiny pores connected to each other and turned into large pores, which were unstable but could not easily return to the original state. The lower the freezing temperature, the greater the destructivity of the soil particles. The increased void ratio led to a weakening effect on the macroscopic mechanical properties.

During the dynamic loading process, the dynamic stress formed a stress concentration in the weakening zone; then, the soil particles slipped and the soil structure was further destroyed. The pressure borne by the skeleton structure transferred to the pore water and caused a rapid accumulation of pore water pressure. At the same time, the development of axial strain reflected the compaction effect from cyclic loading on soil samples. It could be seen that the microstructural changes of soft soil were correlated with the macroscopic dynamic characteristics under freeze–thaw cycles and cyclic loading. It is demonstrated that the change of macroscopic mechanism was related to the microstructure recombination.

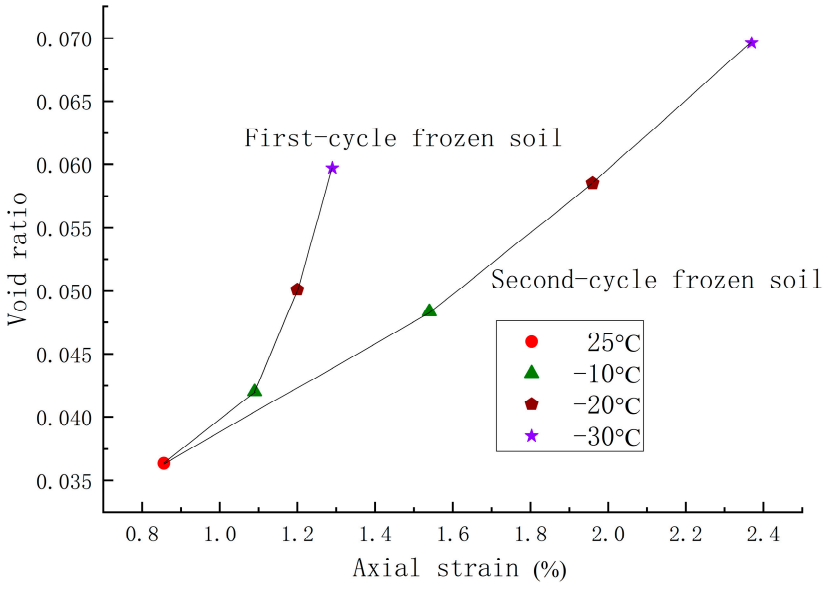

Figure 19. Void ratio vs. axial strain curve.

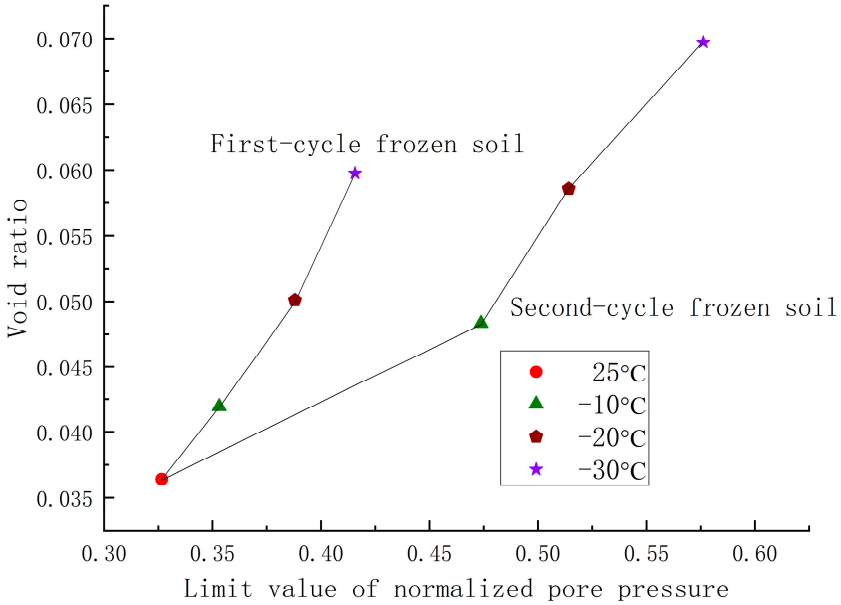

Figure 20. Void ratio vs. limit value of normalized pore pressure curve.

5.2. Relationship of Void Ratio Change and Axial Strain

The weakening mechanism of soft soil was closely related to the change of the microstructure. In essence, the macroscopic strain derived from the redistribution of the microstructure. Figures 21 and 22 show the changes for the first-cycle frozen soil and second-cycle frozen soil under cyclic loading at freezing temperatures of −10 °C, −20 °C, and −30 °C. From the curve of the percentage changes of the void ratio and limit value of normalized pore pressure, it can be seen that the axial strain and pore pressure both increase with the rise of the void ratio decrement.

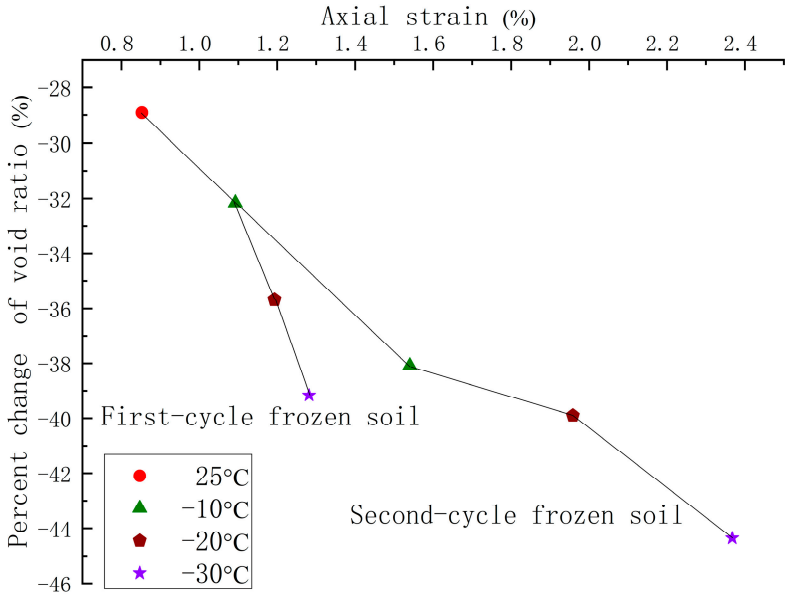

Figure 21. Percentage change of the void ratio vs. axial strain curve.

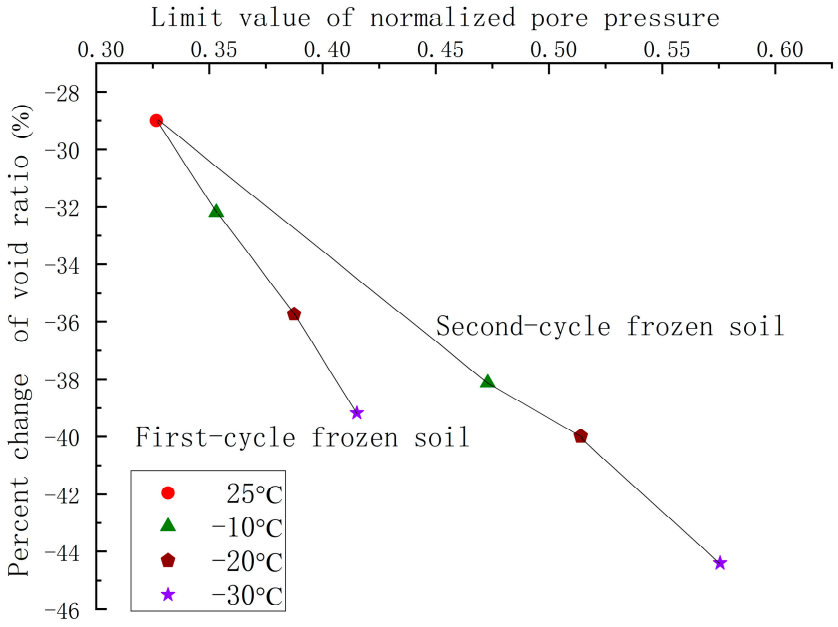

Figure 22. Percentage change of the void ratio curve vs. limit value of normalized pore pressure.

The sharp rise of the soil voids under the freeze–thaw cycle provided a large settling volume for the final settlement. The effect of cyclic loading was a process of energy accumulation; at the beginning of loading, the larger pores were squeezed, and so the soil structure underwent a compaction tendency. When the external load broke the balance of attractive and repulsive forces between the water and grains, a relative slip occurred because of the destroyed junctions between the soil particles. At the same time, the proportion of external load that the pore water carried increased. The compacting effect became more significant as the rate of excess pore pressure and axial strain accumulation increased in speed.

As the cyclic loading was applied, the adjacent structural elements moved gradually closer together, and the loosely-bound water was squeezed out. After that, it was difficult for the adjacent structural elements to move further under the attraction of strongly-bound water. Then, the rate of axial strain and pore pressure growth slowed down and gradually stabilized so that the structure reached a new equilibrium state. For the soil, the lower the freezing temperature, the greater the damage to the structure was. In other words, the lower the freeze temperature or the larger the number of freeze–thaw cycles, the less energy is required for particle rearrangement from cyclic loading.

6. Conclusions

From the experiment, we analyzed the weakening mechanism of the frozen–thawed soil under cyclic loading from the microscopic point of view. Five conclusions are obtained from the preceding study.

- After freeze–thaw cycles, the flaky structure in the soil sample sharply increased. The increment became more and more significant with the increase of the freeze–thaw cycle number and the decrease of temperature. Because of the freeze–thaw cycle, the number of tiny pores ($D < 0.5$ μm) decreased, while the number of large pores ($D \geq 1$ μm) increased, and so the void ratio also rose. Under a temperature of below zero, the complexity structure of pores became more complex, indicating the average fractal dimension of the pores increased.
- After loading, the number of large pores were reduced, resulting in a decrease in the porosity ratio. The shift of the cumulative distribution curves indicated that the proportion of tiny pores increased and the proportion of large pores decreased, so that the structure became denser.

- At the beginning of cyclic loading, the accumulated energy of the external load exceeded the binding energy of the partial soil particles. Then, the proportion of the external load that the pore water bore was increased due to the displacement of the particles, resulting in a faster accumulation rate of excess pore pressure.
- After cyclic loading, the soil skeleton unit was gradually steadied, and the squeezing effect of the soil was reduced. At this time, the soil structure reached a stable state, shown as a reduction in the accumulation of excess pore pressure and axial strain.

Author Contributions: Conceptualization, Z.D. and B.K.; formal analysis, B.K.; investigation, B.X. and F.Z.; resources, M.Z.; writing—original draft preparation, B.K.; writing—review and editing, Z.D.; supervision, X.W.; funding acquisition, Z.D.

Funding: This work is supported by the Chinese National Natural Science Foundation (51508506), the financial support from the Zhejiang Natural Science Foundation (LQ16E080008), Hangzhou Science and Technology Plan Project (20172016A06, 20160533B94, 20180533B06, 20180533B12), Zhejiang University City College Scientific Research Foundation (No. JZD18003).

Conflicts of Interest: The authors declare no conflict of interest.

References

1. Wu, X.; Jin, S.; Chang, L. Monitoring bare soil freeze–thaw process using GPS-interferometric reflectometry: Simulation and validation. *Remote Sens.* **2017**, *10*, 14. [CrossRef]
2. Jadoon, K.Z.; Weihermüller, L.; McCabe, M.F.; Moghadas, D.; Vereecken, H.; Lambot, S. Temporal monitoring of the soil freeze-thaw cycles over a snow-covered surface by using air-launched ground-penetrating radar. *Remote Sens.* **2015**, *7*, 12041–12056. [CrossRef]
3. Jagdhuber, T.; Stockamp, J.; Hajnsek, I.; Ludwig, R. Identification of soil freezing and thawing states using SAR polarimetry at C-band. *Remote Sens.* **2014**, *6*, 2008–2023. [CrossRef]
4. Zhao, Z.; Shen, R.; Feng, W.; Zhang, Y.; Zhang, Y. Soil thermal balance analysis for a ground source heat pump system in a hot-summer and cold-winter region. *Energies* **2018**, *11*, 1206. [CrossRef]
5. Miao, C.; Chen, J.; Zheng, X.; Zhang, Y.; Xu, Y.; Du, Q. Soil water and phreatic evaporation in shallow groundwater during a freeze-thaw period. *Water* **2017**, *9*, 396. [CrossRef]
6. Bing, H.; He, P.; Zhang, Y. Cyclic freeze-thaw as a mechanism for water and salt migration in soil. *Environ. Earth Sci.* **2015**, *74*, 675–681. [CrossRef]
7. Wang, Y.; Yang, J.; Chen, Y.; Wang, A.; Maeyer, P.D. The spatiotemporal response of soil moisture to precipitation and temperature changes in an arid region, China. *Remote Sens.* **2018**, *10*, 468. [CrossRef]
8. Zwieback, S.; Paulik, C.; Wagner, W. Frozen soil detection based on advanced scatterometer observations and air temperature data as part of soil moisture retrieval. *Remote Sens.* **2015**, *7*, 3206–3231. [CrossRef]
9. Hua, W.; Wang, C.; Chen, G.; Yang, H.; Zhai, Y. Measurement and simulation of soil water contents in an experimental field in delta plain. *Water* **2017**, *9*, 947. [CrossRef]
10. Tao, G.; Chen, Y.; Kong, L.; Xiao, H.; Chen, Q.; Xia, Y.A. Simple fractal-based model for soil-water characteristic curves incorporating effects of initial void ratios. *Energies* **2018**, *11*, 1419. [CrossRef]
11. Feng, H.; Chen, J.; Zheng, X.; Xue, J.; Miao, C.; Du, Q.; Xu, Y. Effect of sand mulches of different particle sizes on soil evaporation during the freeze-thaw period. *Water* **2018**, *10*, 536. [CrossRef]
12. Zhai, C.; Wu, S.; Liu, S.; Qin, L.; Xu, J. Experimental study on coal pore structure deterioration under freeze–thaw cycles. *Environ. Earth Sci.* **2017**, *76*, 507. [CrossRef]
13. Watanabe, K.; Kugisaki, Y. Effect of macropores on soil freezing and thawing with infiltration. *Hydrol. Process.* **2017**, *31*, 270–278. [CrossRef]
14. Leroueil, S.; Tardif, J.; Roy, M.; Rochelle, P.L.; Konrad, J.M. Effects of frost on the mechanical behaviour of Champlain Sea clays. *Can. Geotech. J.* **1991**, *28*, 690–697. [CrossRef]
15. Chamberlain, E.J.; Gow, A.J. Effect of freezing and thawing on the permeability and structure of soils. *Eng. Geol.* **1979**, *13*, 73–92. [CrossRef]
16. Chamberlain, E.J. Effect of freeze-thaw cycles on the permeability and macrostructure of soils. *Cold Reg. Res. Eng. Lab.* **1990**, *90*, 145–155.
17. Viklander, P. Permeability and volumxe changes in till due to cyclic freeze/thaw. *Can. Geotech. J.* **1998**, *35*, 471–477. [CrossRef]

18. Sangrey, D.A.; Henkel, D.J.; Esrig, M.I. The effective stress response of a normally consolidated clay. *Soils Found.* **1969**, *22*, 77–91.
19. Zhao, Y.; Si, B.; He, H.; Xu, J.; Peth, S.; Horn, R. Modeling of coupled water and heat transfer in freezing and thawing soils, Inner Mongolia. *Water* **2016**, *8*, 424. [CrossRef]
20. Zhou, J.; Tang, Y. Artificial ground freezing of fully saturated mucky clay: Thawing problem by centrifuge modeling. *Cold Reg. Sci. Technol.* **2015**, *117*, 1–11. [CrossRef]
21. He, P.P.; Cui, Z.D. Dynamic response of a thawing soil around the tunnel under the vibration load of subway. *Environ. Earth Sci.* **2015**, *73*, 2473–2482. [CrossRef]
22. Sheahan, T.C.; Ladd, C.C.; Germaine, J.T. Rate-dependent undrained shear behavior of saturated clay. *J. Geotech. Eng.* **1996**, *122*, 99–108. [CrossRef]
23. Graham, J.; Au, V.C.S. Effects of freeze-thaw and softening on a natural clay at low stresses. *Can. Geotech. J.* **2011**, *22*, 69–78. [CrossRef]
24. Kazuya, K.; Yamanouchi, T.; Hirao, K. Cyclic strength and deformation of normally consolidated clay. *Soils Found.* **1982**, *22*, 77–79.
25. Larew, H.G.; Leonards, G.A. A strength criterion for repeated loads. *Highw. Res. Board Proc.* **1962**, *41*, 529–566.
26. Zhang, Z.L.; Cui, Z.D. Analysis of microscopic pore structures of the silty clay before and after freezing-thawing under the subway vibration loading. *Environ. Earth Sci.* **2017**, *76*, 528. [CrossRef]
27. Pirastru, M.; Marrosu, R.; Prima, S.D.; Keesstra, S.; Giadrossich, F.; Niedda, M. Lateral saturated hydraulic conductivity of soil horizons evaluated in large-volume soil monoliths. *Water* **2017**, *9*, 862. [CrossRef]
28. Fu, Q.; Hou, R.; Li, T.; Yan, P.; Ma, Z. The critical depth of freeze-thaw soil under different types of snow cover. *Water* **2017**, *9*, 370.
29. Lv, S.; Zeng, Y.; Wen, J.; Zhao, H.; Su, Z. Estimation of penetration depth from soil effective temperature in microwave radiometry. *Remote Sens.* **2018**, *10*, 519. [CrossRef]
30. Xia, H.; Cao, Y.M.; De Roeck, G. Theoretical modeling and characteristic analysis of moving-train induced ground vibrations. *J. Sound Vib.* **2010**, *329*, 819–832. [CrossRef]
31. Jung, A.; Vohland, M.; Thielebruhn, S. Use of a portable camera for proximal soil sensing with hyperspectral image data. *Remote Sens.* **2015**, *7*, 11434–11448. [CrossRef]
32. Kolay, E. Modeling the effect of freezing and thawing for sedimentary rocks. *Environ. Earth Sci.* **2016**, *75*, 210. [CrossRef]